

PNNL-33544

# **Fusion Blanket and Fuel Cycle Research at PNNL**

FY22 Year-end Report

October 2022

Wahyu Setyawan Weilin Jiang David J. Senor



#### **DISCLAIMER**

This report was prepared as an account of work sponsored by an agency of the United States Government. Neither the United States Government nor any agency thereof, nor Battelle Memorial Institute, nor any of their employees, makes any warranty, express or implied, or assumes any legal liability or responsibility for the accuracy, completeness, or usefulness of any information, apparatus, product, or process disclosed, or represents that its use would not infringe privately owned rights. Reference herein to any specific commercial product, process, or service by trade name, trademark, manufacturer, or otherwise does not necessarily constitute or imply its endorsement, recommendation, or favoring by the United States Government or any agency thereof, or Battelle Memorial Institute. The views and opinions of authors expressed herein do not necessarily state or reflect those of the United States Government or any agency thereof.

PACIFIC NORTHWEST NATIONAL LABORATORY

operated by

BATTELLE

for the

UNITED STATES DEPARTMENT OF ENERGY

under Contract DE-AC05-76RL01830

Printed in the United States of America

Available to DOE and DOE contractors from the Office of Scientific and Technical Information, P.O. Box 62, Oak Ridge, TN 37831-0062

www.osti.gov ph: (865) 576-8401 fox: (865) 576-5728 email: reports@osti.gov

Available to the public from the National Technical Information Service 5301 Shawnee Rd., Alexandria, VA 22312 ph: (800) 553-NTIS (6847) or (703) 605-6000

email: <a href="mailto:info@ntis.gov">info@ntis.gov</a>
Online ordering: <a href="mailto:http://www.ntis.gov">http://www.ntis.gov</a>

#### 1.0 Introduction

During the reporting period, research at PNNL focused on two tasks within the DOE Fusion Blanket and Fuel Cycle Program. Research on Task 1, Tritium Extraction from Pb-Li and He Using a Vacuum Permeator, focused on atomistic modeling to better understand tritium transport in Pd-coated V vacuum permeators. As a lower cost alternative to Pd permeators, thin coatings of Pd (or other noble metals) can be deposited over a substrate like V. However, the permeation performance of composite metal membranes degrades over time, due to the formation of intermetallics at the coating-substrate interface. Computational studies were performed to better understand tritium transport through these Pd-V intermetallics. The results of the FY22 Pd-V modeling study were recently submitted for publication in *Computational Materials Science* (Setyawan and Senor 2022a) and presented at the Technology of Fusion Energy conference (Setyawan and Senor 2022b). Future work in this area will focus on interdiffusion barriers to prevent intermetallic formation that is deleterious to tritium transport. There are opportunities for collaboration with researchers at the Colorado School of Mines, who are manufacturing and testing candidate interdiffusion barriers.

Research on Task 3, Solid Breeder Materials, included ion irradiation and post-irradiation characterization of lithium orthosilicate (Li<sub>2</sub>SiO<sub>4</sub>) and lithium metasilicate (Li<sub>2</sub>SiO<sub>3</sub>) to improve fundamental understanding of irradiation effects, in combination with atomistic modeling focused on the energetics of He clustering in these two ceramic phases. The results of the study suggested that the Li<sub>4</sub>SiO<sub>4</sub> phase, which is more desirable as a solid breeder due to its higher Li density, was amorphized during ion irradiation while the Li<sub>2</sub>SiO<sub>3</sub> phase appeared to be more resistant to irradiation damage. It is possible that Li loss contributed to the poor irradiation performance of the Li<sub>4</sub>SiO<sub>4</sub>, and some thoughts are provided regarding coatings that could be applied to solid breeders like this to prevent Li loss at elevated temperature while not hindering tritium diffusion. The results of the FY22 ion irradiation study were recently submitted for publication in *Journal of Nuclear Materials* (Jiang et al. 2022a) and presented at the 22<sup>nd</sup> International Conference on Ion Beam Modification of Materials (Jiang et al. 2022b). Future work in this area will focus on Li-rich ceramics such as Li<sub>5</sub>AlO<sub>4</sub> and Li<sub>8</sub>ZrO<sub>6</sub> that have high Li density and should provide rapid tritium release based on previous work with less Li-rich ceramics (Jiang et al. 2017a, Jiang et al. 2017b, Jiang et al. 2020).

# 2.0 Task 1 – Tritium Diffusion in Pd/V Vacuum Permeators

In FY22, density functional theory (DFT) studies were continued to understand detrimental phenomena that influence tritium permeation in a Pd/V vacuum permeator membrane. Experiments by Edlund and McCarthy (1995) showed a severe reduction of hydrogen flux through a Pd/V membrane over time and cross-sectional analyses after permeation experiments revealed an extensive interdiffusion region. Intermetallic compounds are likely to form in the interdiffusion region, even though, to our knowledge, the crystalline phases in this region have never been characterized experimentally. To elucidate if intermetallic compounds directly inhibit tritium permeation, we employ DFT to calculate the permeability of tritium in several Pd-V compounds.

First-principles calculations of the Pd-V phase diagram have predicted five stable compounds, namely Pd<sub>8</sub>V (tI18),  $\beta$ -Pd<sub>3</sub>V (tI8),  $\alpha$ -Pd<sub>2</sub>V (oI6), PdV<sub>3</sub> (cP8), and PdV<sub>4</sub> (tI10). Three of them,  $\beta$ -Pd<sub>3</sub>V,  $\alpha$ -Pd<sub>2</sub>V, and PdV<sub>3</sub>, have been observed experimentally. For the present study, three phases are selected, namely Pd<sub>8</sub>V (the phase with the closest composition to Pd metal),  $\alpha$ -Pd<sub>2</sub>V (near the middle of the composition range and the most stable phase), and PdV<sub>4</sub> (the phase with the closest composition to V). The bulk of the DFT calculations of formation and migration energies (for each migration hop) for tritium

was done in FY21 (Jiang et al. 2021). In FY22, a MATLAB script was developed to calculate the overall migration energy for a given path that consists of multiple hops. The script allows more paths, across the compound's unit cell, to be easily explored to find the optimum one. In addition to tritium, a similar analysis for protium and deuterium is done.

The results show that Pd-V compounds do not readily absorb H, D, or T at interstitial sites as evidenced by positive formation energies in most of the sites. The only site with a negative formation energy is in the most stable site in Pd<sub>8</sub>V, with a formation energy of -0.07 eV for H, and -0.05 eV for D and T. In  $\alpha$ -Pd<sub>2</sub>V, the most stable site shows a formation energy of 0.09 eV for all isotopes, while in PdV<sub>4</sub>, the formation energy at the most stable site is 0.07 eV (H), 0.03 eV (D), and 0.02 eV (T). All the formation energies in these compounds are higher than those in Pd (-0.13 eV for H, -0.12 eV for D and T) and V (-0.33 eV for H, -0.22 eV for D, and -0.27 eV for T). The results suggest the solubility of hydrogen isotopes in Pd-V compounds is lower than in the pure metals. Furthermore, the compound near the middle of the composition range (the  $\alpha$ -Pd<sub>2</sub>V) has the least solubility. A similar trend is observed on the migration energies, with  $\alpha$ -Pd<sub>2</sub>V showing the highest migration energies. The trend in the formation and migration energy indicates that the permeability (the product of solubility and diffusivity) of the compounds is even lower than that of Pd and V. Table 2.1 summarizes the overall migration energy across a unit cell of each compound along x, y, and z dimensions, for H, D, and T.

**Table 2.1.** DFT calculated formation energy  $(E_f)$  of hydrogen isotopes (H, D, and T) at the most stable interstitial site in Pd-V intermetallic phases, Pd, and V, and the overall migration energy  $(E_m)$  of the easiest migration path across a unit cell for these isotopes along x, y, and z dimensions. Energies are given in eV.

	Pd (fcc)	Pd <sub>8</sub> V (tI18)	$\alpha$ -Pd <sub>2</sub> V (oI6)	PdV <sub>4</sub> (tI10)	V (bcc)
$E_f[H]$	-0.13	-0.07	0.09	0.07	-0.22
$E_{m,x}$ [H]	0.22	0.48	0.46	0.38	0.01
$E_{m,y}$ [H]	0.22	0.48	0.36	0.38	0.01
$E_{m,z}$ [H]	0.22	0.28	0.53	0.29	0.01
$E_f[D]$	-0.12	-0.05	0.09	0.03	-0.25
$E_{m,x}$ [D]	0.21	0.45	0.45	0.40	0.04
$E_{m,y}$ [D]	0.21	0.45	0.35	0.40	0.04
$E_{m,z}$ [D]	0.21	0.25	0.52	0.30	0.04
$E_f[T]$	-0.12	-0.05	0.09	0.02	-0.27
$E_{m,x}[T]$	0.20	0.44	0.45	0.40	0.06
$E_{m,y}$ [T]	0.20	0.44	0.35	0.40	0.06
$E_{m,z}$ [T]	0.20	0.24	0.52	0.30	0.06

Based on the parameters in Table 2.1, the ratio of permeabilities of hydrogen isotopes in the intermetallic phases to their permeabilities in Pd and V metals were calculated. Figure 2.1 shows the permeability ratios as a function of temperature. For tritium in the least permeable compound ( $\alpha$ -Pd<sub>2</sub>V), the permeability at 400 °C is 10<sup>-3</sup> times lower than in Pd, and 5×10<sup>-6</sup> times lower than in V. Permeation ratios for H and D are similar to those for T. The calculations strongly suggest that intermetallic compounds significantly inhibit the permeation of H, D, and T. Furthermore, the effect is more severe at lower temperatures. A paper has been submitted to *Computational Materials Science* to report this study.

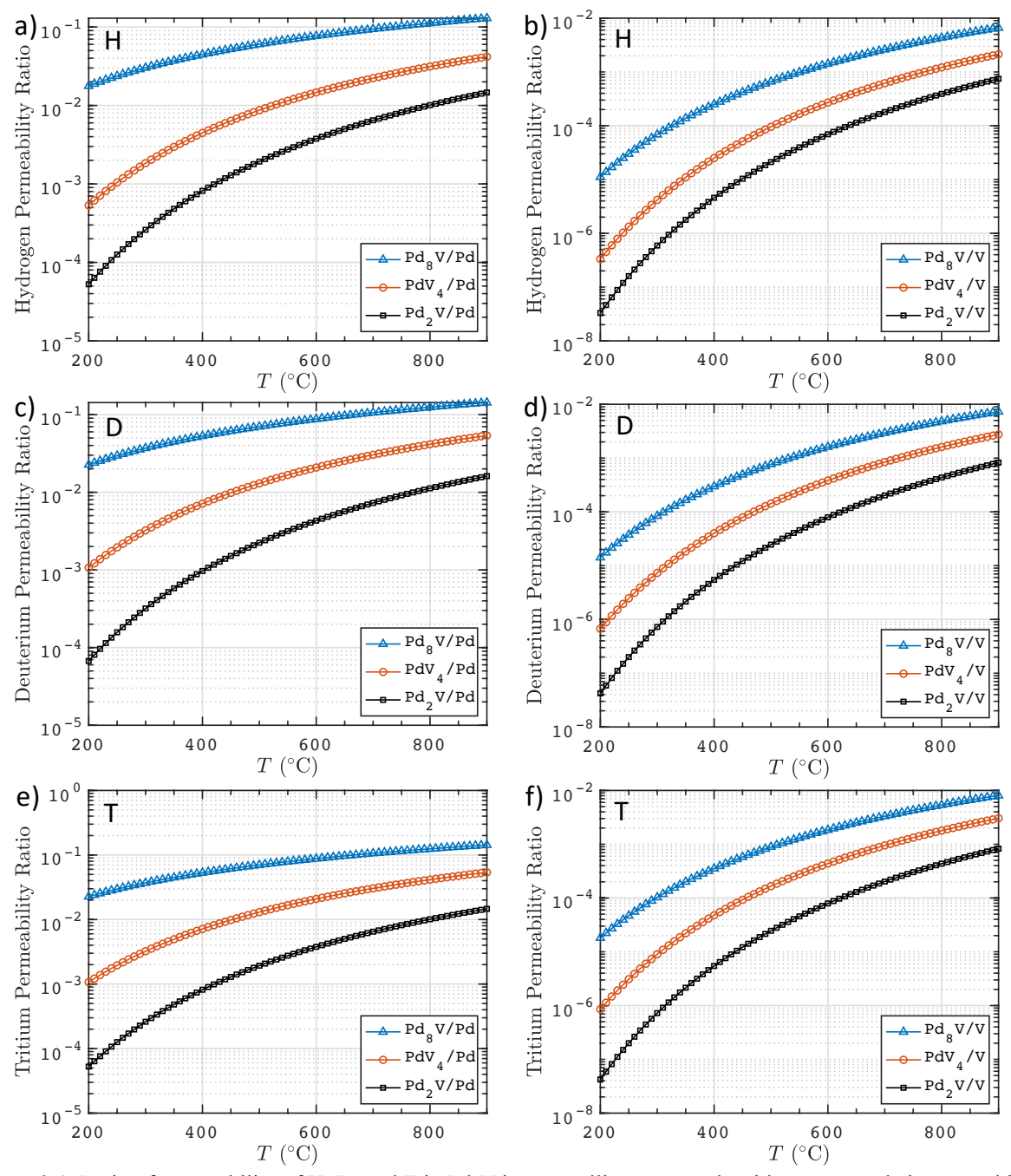


**Figure 2.1.** Ratio of permeability of H, D, and T in Pd-V intermetallic compounds with respect to their permeability in Pd and V, plotted as a function of temperature.

In the future, interdiffusion barrier layers that are suitable for Pd/V membrane will be explored via similar modeling studies, in collaboration with the ARPA-E project at Colorado School of Mines in which candidate interdiffusion barrier layers are being fabricated and tested. In addition, a time-dependent tritium permeation model through a permeator membrane will be developed using the TMAP8 code, firstly applied to the Pd/V membrane based on the atomistic data that have been gathered in FY21 and FY22. The model will be useful to evaluate how long a membrane can be effectively used for a given operating temperature.

# 3.0 Task 3 – Microstructural Evolution in Li<sub>4</sub>SiO<sub>4</sub> and Li<sub>2</sub>SiO<sub>3</sub>

#### 3.1 Ion Irradiation

As described in the PNNL FY21 annual report (Jiang et al. 2021), the crystalline phase  $Li_2SiO_3$  was identified in an ion irradiated region of a  $Li_4SiO_4/Li_2SiO_3$  pellet (Sample T4-4). However, the crystalline phase of  $Li_4SiO_4$  was never observed even though it was present in higher volume fraction than  $Li_2SiO_3$  in the pellet. In addition, while ceramics with a high Li density offer advantages for tritium blanket applications, including high-yield tritium production and fast tritium transport, they are generally expected to have high lithium volatility during irradiation at elevated temperatures. This is because Li atoms or interstitials created by the irradiation have a high mobility in the irradiation-damaged lattice. This behavior has been observed in  $Li_4SiO_4/Li_2SiO_3$  and  $\gamma$ -LiAlO<sub>2</sub> pellets from recent studies (Jiang et al. 2022, Jiang et al. 2017a, Jiang et al. 2017b). To prevent a significant Li loss without greatly suppressing tritium release, there is a need to perform further investigations. This report intends to address the issues associated with both the missing  $Li_4SiO_4$  phase and Li loss. A plan for the near-term study is also provided.

Sequential ion irradiation was performed on  $Li_4SiO_4/Li_2SiO_3$  pellets with 2.50 MeV  $Si^+$ , 62 keV  $He^+$  and 40 keV  $D^+$  ions. Sample T4-2 was irradiated to  $8.2\times10^{16}$   $Si^+/cm^2$ ,  $3.7\times10^{16}$   $He^+/cm^2$  and  $2.9\times10^{16}$   $D^+/cm^2$  at room temperature; Samples T4-1 and T4-3 to the same fluences at 300 and 500°C, respectively. Subject to the error from SRIM13 simulations, the dpa and gas species concentrations around the depth of 500 nm in an ion irradiated  $Li_4SiO_4$  grain are comparable to those in the material after one year irradiation in the SlimCS DEMO fusion reactor. Sample T4-4 was irradiated to twice the fluence of each ion species at 500°C. While deuterium (D) is used as a surrogate for tritium (T), self-ion (Si<sup>+</sup>) is employed to emulate high-energy neutron irradiation.

A number of methods have been employed to search for the Li<sub>4</sub>SiO<sub>4</sub> phase in the ion irradiated pellets. First, electron backscatter diffraction (EBSD) was attempted. It was found that whisker-like protrusions were formed on a Li<sub>4</sub>SiO<sub>4</sub>/Li<sub>2</sub>SiO<sub>3</sub> pellet after less than 10 min exposure to a 20 keV electron beam at a current of 45 nA under an SEM, as shown in Figure 3.1(a), likely due to electron irradiationinduced material decomposition. This behavior does not allow EBSD to index the surface grains, Energy dispersive spectroscopy (EDS) mapping was also applied at a low energy of 2 keV using the Oxford Light Element EDS Detector. The use of the low electron energy was to minimize the material damage. The Li  $K_{\alpha}$  x-ray line (54.3 eV) is located between the edges of the Si L<sub>2</sub> & L<sub>3</sub> lines (~100 eV) and a noise peak  $(\sim 0 \text{ eV})$ , as shown in Figure 3.1(b). As a result, the relatively weak Li peak cannot be resolved from these two surrounding peaks. In addition, a traditional EDS Ultim Max Detector was used to determine the Si/O atomic ratios in grains with different contrasts that were exhibited in a backscattered electron (BSE) image, followed by FIB preparation of a transmission electron microscopy (TEM) specimen at a selected grain with a Si/O atomic ratio close to 0.25 (the ratio for Li<sub>4</sub>SiO<sub>4</sub>) for electron diffraction under a TEM microscope. The result shows that the selected grain was fully amorphized (data not shown). The final search for the Li<sub>4</sub>SiO<sub>4</sub> phase was performed in an unirradiated pellet (Sample T4-9), where polycrystalline grains of both Li<sub>2</sub>SiO<sub>3</sub> and Li<sub>4</sub>SiO<sub>4</sub> phases were observed (data not shown). A deep region in Sample T4-4 was also examined. Figure 3.2 shows a low-magnification TEM image, a diffraction pattern from a region at the depth of ~3 µm (unirradiated), and a simulated electron diffraction pattern for [001] oriented Li<sub>4</sub>SiO<sub>4</sub>. Both the lattice symmetry and diffraction intensities between the experiment and simulation match very well. The observed values of the interplanar spacing are 0.319 nm for d(100) and 0.534 nm for  $d(0\overline{2}0)$ , which also agree reasonably well with the simulation within 0.7% and 4%, respectively. The data indicate that the grain is most likely a single crystal Li<sub>4</sub>SiO<sub>4</sub> with the [001] orientation. However, similar crystalline Li<sub>4</sub>SiO<sub>4</sub> phases have never been observed in the irradiated region (depth < 1.5 um). It is likely that the Li<sub>4</sub>SiO<sub>4</sub> phase was fully amorphized under the irradiation conditions of this study. As the

Li<sub>2</sub>SiO<sub>3</sub> phase remains crystalline under the same irradiation conditions, it is likely that Li<sub>2</sub>SiO<sub>3</sub> is more resistant to irradiation-induced full amorphization than Li<sub>4</sub>SiO<sub>4</sub>.

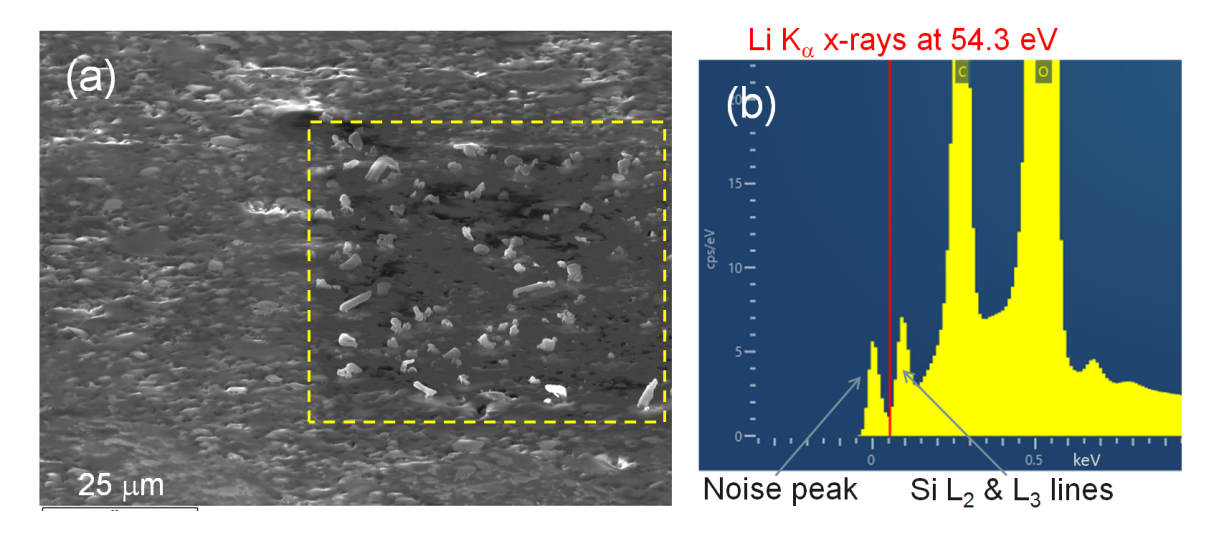


**Figure 3.1.** (a) Whisker formation on a Li<sub>4</sub>SiO<sub>4</sub>/Li<sub>2</sub>SiO<sub>3</sub> pellet and (b) light-element EDS spectrum from a Li<sub>4</sub>SiO<sub>4</sub>/Li<sub>2</sub>SiO<sub>3</sub> pellet.

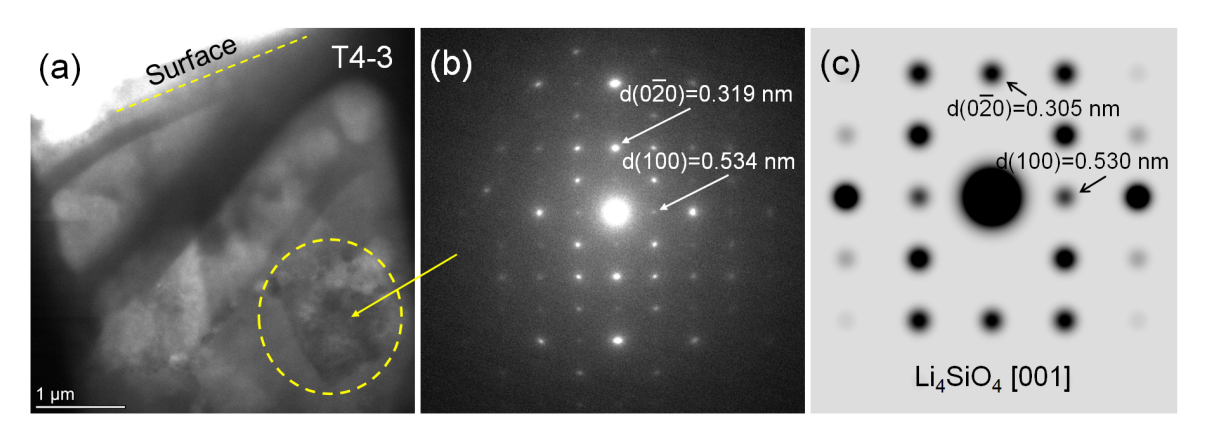


**Figure 3.2.** (a) A low-magnification TEM image of sample T4-3, (b) electron diffraction pattern in an unirradiated area, and (c) simulated diffraction pattern for [001] oriented Li<sub>4</sub>SiO<sub>4</sub>.

In order to minimize Li loss without significantly suppressing tritium release from Li ceramics during neutron irradiation at elevated temperatures, coating Li ceramics with a suitable material may be one of the options that deserve considering. The coating material must have a high diffusivity and low retention for tritium and at the same time can encapsulate Li to a large extent. Obviously, substantial R&D efforts are needed to identify and select the material for application. Previous studies (Jiang and Senor 2020a, Jiang and Senor 2020b) reported D and Li diffusion behavior in high-purity nickel (4N5 from ESPI Metals). 1.50 MeV Ni<sup>+</sup> self-ion irradiation to  $3\times10^{15}$  Ni<sup>+</sup>/cm<sup>2</sup> (10.7 dpa at 384 nm) was first performed at  $300^{\circ}$ C to emulate high-energy neutron irradiation that produces lattice damage without introducing impurities. The irradiated samples were further irradiated at  $300^{\circ}$ C with either  $102 \text{ keV } D_2^+$  ions to  $2\times10^{17}$  D<sup>+</sup>/cm<sup>2</sup> (10.4 at.% D at peak) or 1.57 MeV Li<sup>+</sup> ions to  $2\times10^{15}$  Li<sup>+</sup>/cm<sup>2</sup> (0.083 at.% Li at peak) with a 3.0  $\mu$ m thick Al foil in front of the sample. ToF-SIMS measurements were performed for D depth profiles in nickel with the results shown in Figure 3.3(a). The data indicate that D retention in Ni is

extremely low with a yield comparable to the background level. Thus, a nearly complete release of D from Ni occurred during  $D_2^+$  ion irradiation at 300°C. Evidently, D atoms (and T atoms by inference) have a high diffusivity and low retention in nickel at 300°C. In a sharp contrast, Li concentration shows a well-defined peak with much higher retention of Li than D in Ni even at the peak concentration of two orders of magnitude lower, as shown in Figure 3(b). The data suggest that Li diffusion to a large depth in Ni during Li<sup>+</sup> ion irradiation at 300°C is greatly suppressed. Further investigations of Ni and other relevant materials are needed to emulate their irradiation response in fusion environments, including interfacial behavior and D diffusion and release at higher temperatures.

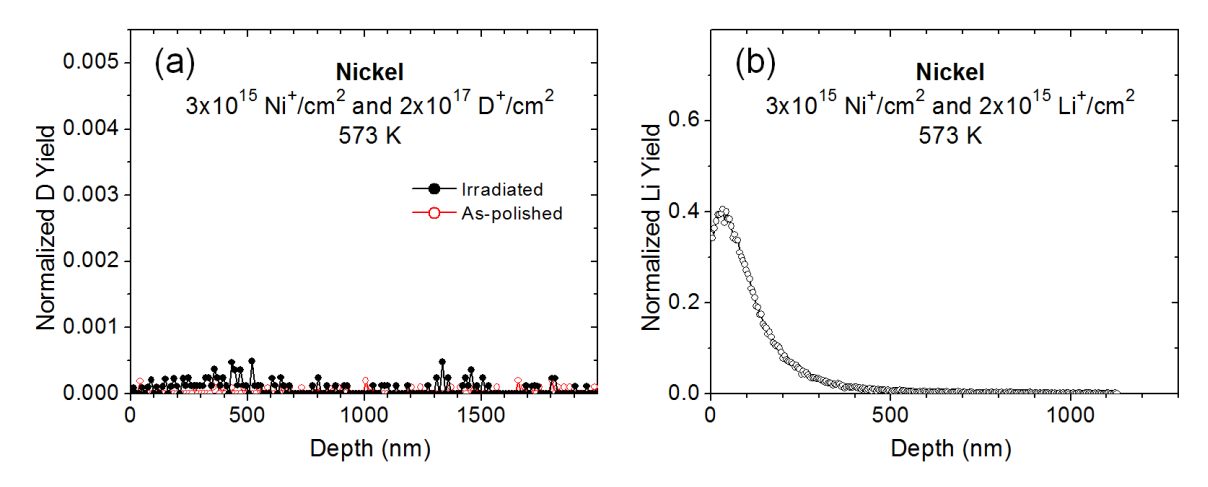


**Figure 3.3.** ToF-SIMS depth profiles of the normalized yields of (a) deuterium and (b) lithium in pure nickel irradiated with Ni<sup>+</sup> self-ions, followed by implantation of D<sub>2</sub><sup>+</sup> or Li<sup>+</sup> ions at 573 K.

Work will continue on the ion irradiation study of ceramic materials with a high Li density. Two candidate compositions of Li<sub>5</sub>AlO<sub>4</sub> and Li<sub>8</sub>ZrO<sub>6</sub> are being currently considered. Synthesis of the powders have been reported (Shin-Mura et al. 2018), but commercial products do not appear to be available. Custom order of powders or pellets with a US company may need to be pursued. Alternatively, collaborations with peer researchers may be sought for to obtain materials for this study. Once the powders are obtained, fabrication of Li<sub>5</sub>AlO<sub>4</sub> and/or Li<sub>8</sub>ZrO<sub>6</sub> pellets will proceed using hot-pressing or isostatic pressing at room temperature followed by sintering in air at a high temperature. It has been found that decomposition of the Li<sub>5</sub>AlO<sub>4</sub> and Li<sub>8</sub>ZrO<sub>6</sub> compounds occurs prior to their melting points at 1,047 and 1,336 °C, respectively (Hernandez and Pereslavtsev 2018). Lithium vaporization rates from both materials are high; however, the lithium vaporization rate gradually decreases with the annealing time as the sintered pellet will be covered by a stable, thin layer ( $\gamma$ -LiAlO<sub>2</sub> or Li<sub>6</sub>Zr<sub>2</sub>O<sub>7</sub>) formed during sintering (Shin-Mura et al. 2018). This surface layer on the as-sintered pellet will be removed for ion irradiation. Sequential self-ion, He<sup>+</sup> and D<sub>2</sub><sup>+</sup> ion irradiation at an elevated temperature and characterization of the irradiated samples will follow. The results from this study will be compared to those obtained in FY21 and FY22 from lithium silicates.

# 3.2 Modeling

In FY22, molecular dynamics (MD) simulations were employed to study helium clustering in  $\alpha$ -Li<sub>4</sub>SiO<sub>4</sub> and Li<sub>2</sub>SiO<sub>3</sub> ceramic breeders. Interatomic potentials developed by Pedone et al. (2006) were used for the lithium silicates. He-He interaction was taken from the Tang and Toennies (2003) potential. He-Li interaction was modeled with a Lennard-Jones (LJ) potential that was fitted to DFT interaction

energy (Senff and Burton 1986). The He-O LJ potential and the He-Si Buckingham potential that were used to study He solution and migration in ZrSiO<sub>4</sub> (Grimes et al. 1990, Saadoune and de Leeuw 2009) were used in this study. To study clustering, He atoms were inserted in the middle of the simulation box, in a pristine α-Li<sub>4</sub>SiO<sub>4</sub> crystal, at a rate of 1 He per 5 ps. Insertion simulations are done at 300 K. Figure 3.4 shows the structure after 500 He atoms (~2 at%) have been inserted. He atoms tend to fill in the space between crystalline planes and are not able to cluster. Subsequent annealing up to 700°C shows spreading of He atoms, confirming the non-clustering behavior. In another set of simulations, a small cavity was created by removing one formula unit (4 Li, 1 Si, and 4 O) and inserting He atoms into this cavity. After several He atoms fill in the cavity, subsequent atoms show a similar behavior as before, i.e. no clustering was observed. In these silicates, the crystal consists of interconnected Si-O tetrahedra. Insertion of He atoms distorts the silicate's crystal, but it is not enough to create Si or O Frenkel pairs, presumably because of the strong Si-O bond.

A factor that may influence the inability of He atoms to displace Si or O atoms from their lattice sites is perhaps because there is no region for the Si or O to escape to in a charge-neutral bulk simulation cell. Thus, test simulations were performed in a slab, where He atoms were inserted at a location 2 nm below a free surface. No clustering was observed; in fact, some He atoms were lost to the surface. Similar sets of simulations were performed for Li<sub>2</sub>SiO<sub>3</sub>, and clustering was not observed in that phase either. The results were tested using lithium silicate interatomic potentials developed by Ma et al. (2018). The Ma potentials confirm the no-clustering behavior obtained with the Pedone potentials. On the other hand, the ion irradiations described in Section 3.1 show He cavities formed in the amorphous regions of lithium silicates. In the ion irradiations, displacement damage as well as lithium loss occur, in addition to influx of He. Combining these results, it appears that He atoms do not readily cluster to form a bubble (or He cavity) in these silicates in the absence of displacement damage.

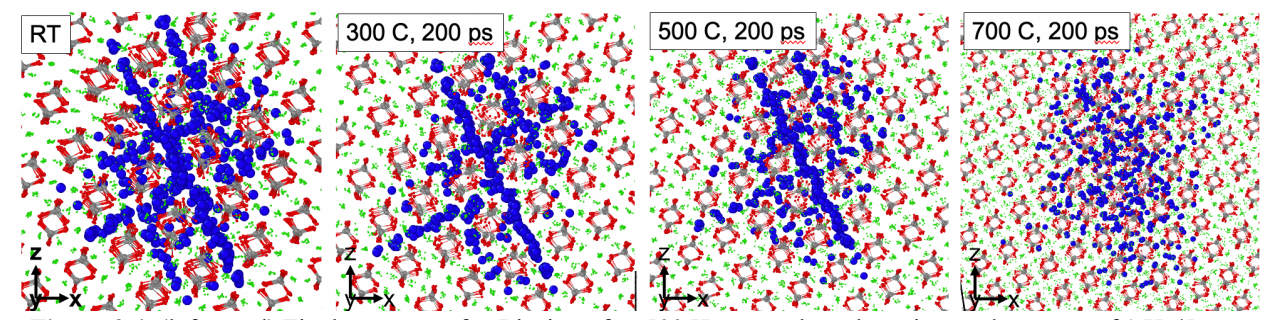


Figure 3.4. (left panel) Final structure of  $\alpha$ -Li<sub>4</sub>SiO<sub>4</sub> after 500 He atoms have been inserted at a rate of 1 He/5 ps at room temperature (RT). Structures after subsequent annealing for 200 ps at 300, 500, and 700°C are shown.

#### 4.0 References

Edlund, DJ, J McCarthy. 1995. "The relationship between intermetallic diffusion and flux decline in composite-metal membranes: implications for achieving long membrane lifetime," *Journal of Membrane Science*, 107:147-153.

Grimes, RW, RH Miller, CRA Catlow. 1990. "The Behavior of Helium in UO<sub>2</sub>: Solution and Migration Energies," *Journal of Nuclear Materials*, 172:123-125.

Hernández, FA, P Pereslavtsev. 2018. "First Principles Review of Options for Tritium Breeder and Neutron Multiplier Materials for Breeding Blankets in Fusion Reactors," *Fusion Engineering and Design*, 137:243-256.

- Jiang, W, J Zhang, DJ Edwards, NR Overman, Z Zhu, L Price, J Gigax, E Castanon, L Shao, DJ Senor. 2017a. "Nanostructural Evolution and Behavior of H and Li in Ion-Implanted γ-LiAlO<sub>2</sub>," *Journal of Nuclear Materials*, 494:411-421.
- Jiang, W, J Zhang, L Kovarik, Z Zhu, L Price, J Gigax, E Castanon, X Wang, L Shao and DJ Senor. 2017b. "Irradiation Effects and Hydrogen Behavior in H<sub>2</sub><sup>+</sup> and He<sup>+</sup> Implanted gamma-LiAlO<sub>2</sub> Single Crystals," *Journal of Nuclear Materials*, 484:374-381.
- Jiang, W, T Wang, Y Wang, Z Zhu, L Shao, DJ Senor. 2020. "Deuterium Diffusion in γ-LiAlO<sub>2</sub> Pellets Irradiated with He<sup>+</sup> and D<sub>2</sub><sup>+</sup> Ions," *Journal of Nuclear Materials*, 538:152357.
- Jiang, W., DJ Senor. 2020a. "Diffusion of Deuterium in Ion Irradiated Zircaloy-4 and Nickel," *PNNL-30634*, Pacific Northwest National Laboratory, Richland, WA.
- Jiang, W, DJ Senor. 2020b. "Lithium Diffusion and Retention in Ion Irradiated Zircaloy-4 and Nickel," *PNNL-30674*, Pacific Northwest National Laboratory, Richland, WA.
- Jiang, W, W Setyawan, DJ Senor. 2021. "Fusion Blanket and Fuel Cycle Research at PNNL: FY21 Year-end Report," *PNNL-32147*, Pacific Northwest National Laboratory, Richland, WA.
- Jiang, W, L Kovarik, MG Wirth, Z Zhu, NL Canfield, LM Seymour, LM Bagaasen, ME Bowden, T Varga, NR Overman, Z Hu, L Shao, DJ Senor. 2022a. "Ion Irradiation Study of Lithium Silicates for Fusion Blanket Applications," submitted to *Journal of Nuclear Materials*.
- Jiang, W, L Kovarik, Z Zhu, NL Canfield, LM Bagaasen, D Senor. 2022b. "Ion Irradiation Study of Lithium Silicates for Fusion Blanket Applications," *PNNL-SA-174576*, presented by Weilin Jiang at the 22<sup>nd</sup> International Conference on Ion Beam Modification of Materials (IBMM-2022), Lisbon, Portugal, 10-15 July 2022.
- Ma, SG, XG Kong, SC Li, et al. 2018. "Applying a new Interatomic Potential for the Simulation of Monoclinic and Triclinic Li<sub>4</sub>SiO<sub>4</sub>," *Materials Chemistry and Physics*, 214:548-556.
- Pedone, A, G Malavasi, MC Menziani, AN Cormack, U Segre. 2006. "A New Self-consistent Empirical Interatomic Potential Model for Oxides, Silicates, and Silica-based Glasses," *Journal of Physical Chemistry B*, 110:11780-11795.
- Saadoune, I, NH de Leeuw. 2009. "A Computer Simulation Study of the Accommodation and Diffusion of He in Uranium- and Plutonium-doped Zircon (ZrSiO<sub>4</sub>)," *Geochimica et Cosmochimica Acta*, 73:3880-3893.
- Senff, UE, PG Burton. 1986. "A CEPA2 Investigation of the He-He and He-Li<sup>+</sup> Potential Functions," *Molecular Physics*, 58:637-645.
- Setyawan, W, DJ Senor. 2022a. "Density functional theory study of formation and diffusion of hydrogen, deuterium, and tritium in Pd-V intermetallic compounds," submitted to *Computational Materials Science*.
- Setyawan, W, DJ Senor. 2022b. "Density Functional Theory Study of Tritium Diffusion in Pd/V Vacuum Permeator," *PNNL-SA-174222*, presented by W. Setyawan at Technology of Fusion Energy (TOFE) 2022, Anaheim, CA, 12-16 June 2022.

Shin-Mura, K, S Honda, T Hoshino, K Sasaki, 2018. "Lithium Vaporization Property of Li<sub>8</sub>ZrO<sub>6</sub> and Li<sub>5</sub>AlO<sub>4</sub> as Tritium Breeders," *Fusion Engineering and Design*, 136:869-873.

Tang, KT, JP Toennies. 2003. "The van der Waals Potentials Between all the Rare Gas Atoms from He to Rn," *Journal of Chemical Physics*, 118:4976-4983.

# Pacific Northwest National Laboratory

902 Battelle Boulevard P.O. Box 999 Richland, WA 99354 1-888-375-PNNL (7665)

www.pnnl.gov